Applied Thermal Engineering 217 (2022) 119160

Contents lists available at ScienceDirect

Applied Thermal Engineering

journal homepage: www.elsevier.com/locate/apthermeng

Analysis and modeling of the tip leakage flow on the performance of small-scale turbopumps for ORC applications

Sajjad Zakeralhoseini *, Jürg Schiffmann

Ecole Polytechnique Fédérale de Lausanne (EPFL), Laboratory for Applied Mechanical Design, CH-1015 Lausanne, Switzerland

ARTICLE INFO

Keywords:
ORC
Turbopumps
CFD
Slip factor
Head rise
1D modeling
Neural networks

ABSTRACT

In this paper, the influence of tip clearance on the performance of small-scale turbopumps is studied numerically on extensive parameter ranges suitable for organic Rankine cycle applications. A novel and fully parameterized design model is developed and used to generate a wide range of turbopumps and their fluid domains to carry out three-dimensional computations across the impeller stage. Impellers are investigated at different operating conditions, and the accomplished results are analyzed to characterize the performance at design and off-design conditions. The CFD calculations demonstrate that the slip factor is dependent not only on its geometrical parameters, as considered by most correlations, but also on its operating conditions. The slip factor decreased almost linearly as the flow rate increased. In addition, the tip clearance ratio influences the slip factor, and its influence is non-linear. The head rise decreases as the tip clearance ratios increase. However, for radial impellers, a higher head rise was observed for small tip clearance ratios (<0.10). The numerical data is employed to infer reduced-order models for considering the tip clearance effect in the early-phase design process of small-scale turbopumps. The models predict the CFD data with an average relative deviation of 3.6 % and 5.8 % for the slip factor and the head loss coefficient, respectively.

1. Introduction

Given that 40–50 % of the energy in fuel-driven power generation is usually dissipated [1] employing systems able to recover waste heat is recognized as a promising solution to enhance the efficiency of power generation. A possible way to harness this waste heat can be achieved through the implementation of Organic Rankine Cycles (ORC). ORCs offer exceptional features for exploiting waste heat due to the possibility of a good matching between the temperature profiles of the ORC working fluid and of the waste heat.

The small latent heat of common organic fluids compared to water requires a higher mass flow rate for the same waste heat power, and consequently, the size and power consumption of the pump are increased significantly. Meng et al. [2] investigated an industrial multi-stage centrifugal pump for a specific ORC system for waste heat recovery. The efficiency of the pump is reported to be between 15 % and 65.7 %, which suggests that pump design should be considered in the design process of an ORC system since a low pump efficiency significantly decreases the overall thermal efficiency of ORCs. Landelle et al. [3] studied the performance of a reciprocating pump working with R134a for an ORC system. They showed that the volumetric efficiency of the pump running with organic fluid remained high compared to its design working fluid (water) and to experimental data reported by the manufacturer. Bianchi et al. [4] proposed design considerations and 1D models for sliding vane pumps suitable for small-scale ORC systems. They emphasized the importance of considering pumping power for small-scale ORC systems, which corroborates with the finding by Meng et al. [2].

Positive displacement pumps such as gear and progressive cavity pumps are used for applications that require high-pressure rises and low mass flow rates. Their underlying working principle is suitable for high viscosity fluids (to ensure lubrication), which is not the case for most working fluids used in ORC, which often yield only low viscosity. Centrifugal pumps, on the other hand, provide lower pressure rises and higher mass flow rates, which usually leads to multi-stage designs to achieve the pressure rise specifications of typical ORCs. However, the weight and size of the multi-stage pumps stage can even annihilate the positive effects of installing waste heat recovery on vehicles. Hence, smaller and more efficient pumps are necessary, especially when innovative systems for mobile heat recovery applications must be introduced. One possibility to achieve this objective is to use high-speed

* Corresponding author.
E-mail addresses: sajjad.zakeralhoseini@epfl.ch (S. Zakeralhoseini), jurg.schiffmann@epfl.ch (J. Schiffmann).

https://doi.org/10.1016/j.applthermaleng.2022.119160
Received 1 March 2022; Received in revised form 6 July 2022; Accepted 12 August 2022
Available online 28 August 2022

Nomenclature

B	blade height, m
C	tip clearance gap, m
c	absolute velocity, m/s
H	head, m
m	meridional length, m
L	length of medial axis, m
Q	flow rate, m^3s^{-1}
r	radius, m
u	peripheral velocity, m/s
w	relative velocity, m/s
Z	number of blades
z	axial length
p_S	static pressure, Pa
$p_{T,r}$	reduced stagnation pressure, Pa
C_p	pressure coefficient
n_q	specific speed, rpm, m^3s^{-1}, m
n_s	specific speed, non-dimensional

Greek letters

β	flow angle, °
β_B	blade angle, °
ρ	density, kg m^{-3}
γ	slip factor
ω	rotational speed, rad/s
ϕ	flow coefficient, $\frac{Q}{\omega r^3}$
ψ	head coefficient, $\frac{gH}{\omega^2 r^2}$
η	efficiency

Subscripts

I	input
S	shroud
H	hub
M	meridional component
U	circumferential component
0	shrouded impeller
1	inlet station
2	outlet station
∞	blade congruent flow

Abbreviations

CFD	computational fluid dynamics
NN	neural network
ORC	organic Rankine cycle
LE	leading edge
TE	trailing edge

single-stage turbopumps in ORC systems allowing for a compact design of the energy recovery systems.

ORC systems for waste heat recovery require a combination of low-rated flow and high-pressure rise with smaller geometrical dimensions. Considering internal combustion engines for passenger cars or trucks, a bottoming ORC would typically deliver a net output power ranging from 1 to 20 kW [5,6]. Hence, a turbopump for these applications becomes very small compared to the state-of-the-art. Although classical reduced-order models predict the performance of geometrically similar pumps as a function of specific speed, the turbopump performance is also affected by additional effects such as higher relative roughness and tip clearance, which tend to amplify with geometrical down-scaling. The tip clearance is recognized to yield adverse effects on the performance of centrifugal machines due to the development of secondary flows and due to its influence on the slip. It is, therefore, necessary to predict its influence correctly in the early phase of the design process of a turbopump, in particular for reduced scale applications.

Tip clearance. Wood et al. [7] investigated the influence of tip clearance on the performance of several centrifugal pumps. They reported that unshrouded impellers performed better in terms of cavitation in comparison to shrouded impellers. Their observations suggest that at the best efficiency, the slip increases, and the head coefficient decreases with increasing tip clearance unlike for very small relative tip clearances, higher efficiency can be expected for unshrouded impellers. Pampreen [8] studied scaling effects on the performance of centrifugal compressors. His results suggested that Reynolds stresses outweigh the viscous stress, but the compressor efficiency is more influenced by the tip clearance than by the Reynolds number. The experimental measurements conducted by Block and Runsmdler [9] on a centrifugal compressor indicated that there is no notable influence of tip clearance on mass flow rate and pressure ratio, but the efficiency is decreased with increasing tip clearance. Based on an experimental study on a centrifugal compressor at different Reynolds numbers and tip clearances, Mashimo et al. [10] developed a correlation to estimate the loss pertained to the leakage flow through the tip clearance. Their experiments revealed that the leakage flow loss is dependent on the Reynolds number and increases with increasing Reynolds number. They reported the compressor efficiency dropped around 4 % with an increase of the relative tip clearance from 0.0125 to 0.125. Ishida and Senoo [11] experimentally investigated the pressure distribution along the blade tip region in blowers with the design specific speed (dimensionless) of 0.584 and 0.433. They concluded that the loss induced by the tip clearance occurs mostly in the region where the relative velocity is deaccelerated, and since the entrance region, especially close to the throat, is the region where the highest rate of deacceleration occurs, making this region narrower will lead to a notable performance improvement. Senoo and Ishida [12] extended their investigation to axial blowers and developed a method to estimate the efficiency drop and the pressure loss due to the tip clearance in axial and centrifugal impellers. Their results suggested that the tip clearance loss is induced by the tip leakage flow and the adverse pressure gradient along the shroud. They showed that at small tip clearances, the efficiency drop and the pressure loss are almost proportional to the relative tip clearance. They suggested that while the tip clearance value is the main governing parameter, it is not the only influential one determining the tip clearance losses. In a later study, Senoo and Ishida [13] modified their original estimation method to better predict the performance of centrifugal impellers at off-design conditions by including the variation of the slip coefficient induced by the tip clearance losses. The method was compared with experimental data of different centrifugal compressors and the results showed that the influence of tip clearance on the efficiency deterioration gets smaller as the flow rate is reduced. The same observation was noticed for high-pressure-ratio compressors running at a reduced shaft speed. Engeda and Rautenberg [14] showed that the performance of impellers designed to operate at a medium range of the specific speed is most sensitive to the tip clearance effect. However, a simple dependency between the pressure loss and the specific speed was not observed. Brasz [15] carried out an experimental investigation on an unshrouded centrifugal compressor operating at a rotational Mach number ($u_2/a_0 = 1.39$). The results suggested the non-linear dependency of performance to the relative tip clearance. Additionally, a higher sensitivity at smaller clearances was observed. Ishida et al. [16] examined the estimation method they proposed earlier [12,13] through an experimental investigation of an unshrouded backward impeller. The results suggested that the estimation method can predict the

performance of unshrouded impellers with a good agreement if the proper values of the contraction coefficient of the leakage flow are assumed. The coefficient is introduced to account for the vena contracta phenomenon of the flow passing through the tip clearance. In another study, Ishida et al. [17] experimentally investigated the secondary flow pattern at the outlet of an unshrouded radial and a backswept impeller. They suggest that the secondary flow induced by the tip clearance is due to the shear stress component, which is normal to the blade surface and acts against the adverse pressure gradient. The observation suggested that the relative flow angle is hardly affected by the tip clearance at the outlet of the radial impeller, while it is reduced significantly with increasing the tip clearance in the case of the backswept impeller, therefore suggesting an increased effect on the slip factor.

Goto [18] investigated the formation and interaction of secondary flows inside a mixed-flow pump impeller numerically. The computations implied that the boundary layer at the casing gets thicker in case of a large tip clearance, which results in the formation of a strong vortex inside the main passage and the subsequent deterioration of the main flow field.

Based on three-dimensional CFD simulations, Aknouche [19] developed an estimating model to predict the performance deterioration due to the tip clearance of turbopumps. The model accounts for the tip clearance losses induced by the mixing of the tip leakage with the main flow and the increased blockage caused by the lower streamwise velocity of the leakage flow compared to the main flow. Through a numerical study, Eum and Kang [20] computed and analyzed the loss distribution of a centrifugal compressor at different tip clearances. Based on the results, they identified the suction-shroud corner as the region where possibly the highest loss due to the tip clearance occurs, and they proposed a simple correlation for predicting the specific work reduction due to tip clearance leakage. Similar observations were reported by Tang et al. [21] in a small compressor impeller. They reported that the low-momentum region is moved from the suction-shroud corner to the center of the flow channel as the tip clearance increases, which results in further distortion of the flow field and a subsequent efficiency and pressure drop. Through experimental investigation of six different compressors, Turunen-Saaresti and Jaatinen [22] studied the influence of different design parameters on the efficiency and pressure drop induced by the tip clearance. They reported that no clear relation between the efficiency variation, the specific speed, and the diffusion ratio was observed. Similarly, the influence of design parameters such as the specific speed, the blade number, and the ratio of the blade height was not evident on the pressure ratio. Therefore, it emphasized the necessity of further investigation and analysis of design parameters to improve reduced-order models.

Sun et al. [23] numerically investigated the flow field distortion and the variation of the slip factor due to the tip clearance in a micro centrifugal impeller. They showed that in comparison to shrouded impellers, the flow non-uniformity at the impeller outlet is more significant in the open impeller and implies the necessity of developing the slip factor model for the unshrouded impeller. Recent work by Diehl et al. [24] on small-scale centrifugal compressors showed that the loss induced by the tip clearance is independent of the Reynolds number and that the loss related to the tip leakage scales linearly with the relative tip clearance, even for values up to 15 %.

Since the reduced-order models available in the literature are developed and validated for large-scale turbopumps, the influence of geometric down-scaling is not addressed. Thus, they might lead to impractical or even infeasible designs far from optimum for small-scale applications. Therefore, whether the adoption of such models and tools is still applicable at small scales is a matter of argument, especially when design parameters such as the relative tip clearance, which is one of the most distinct differences between large-scale and small-scale, strongly affect the flow structure inside such machines. The literature review reveals that there is limited research on the influence of tip clearance on the performance of turbopumps, while such influence is more investigated for radial compressors.

Slip factor. Various measurements and theoretical flow analysis in centrifugal impellers highlighted that the flow is not blade-congruent and deviates from the path imposed by blade shape due to the non-uniform velocity profiles and the Coriolis acceleration [25], thus leaving the impeller with an outlet flow angle, β_2 less than the blade-congruent flow angle, $\beta_{2\infty}$. This difference causes the circumferential component of absolute velocity to differ as much as ΔC_{u2} with the value of one-dimensional theory, and therefore changes the velocity triangle at the impeller outlet as depicted inFig. 1.

Based on Euler's equation of turbomachinery, the theoretical head rise of the impeller is strongly related to the change of circumferential component of absolute velocity and, therefore, the deviation of flow angle and the consequence difference of ΔC_{u2} reduces Euler's head rise significantly. The slip factor is defined to consider the flow deviation effects in decreasing energy transmission. The definition of slip factor in this study is defined by Eq. (1):

$$\gamma = 1 - \frac{c_{u2\infty} - c_{u2}}{u_2} \tag{1}$$

where $c_{u2\infty}$ is the circumferential component of absolute velocity for an impeller with an infinite number of blades. The smaller the slip factor, the higher the deviation of flow from the blade. The value of the slip factor usually is between 0.65 and 0.8 at the impeller design point [26] herefore, the error resulting from the one-dimensional analysis is significant. Stepanoff [27] suggested the value of 0.73 for the slip coefficient for pumps.

Due to this significant impact on the performance of centrifugal impellers, the slip factor has been studied by several researchers. However, no model has yet been found to predict the slip factor in general. Busemann [28] introduced two correction coefficients B and C into the dimensionless performance characteristic obtained with one-dimensional theory. The dimensionless performance characteristic represented by the head coefficient ($\psi = \frac{gH}{\omega^2 r^2}$) is stated as:

$$\psi = 1 - \varphi \cot(\beta_{2B}) \tag{2}$$

and the performance characteristic corrected by Busemann [28] is as follows:

$$\psi = B - C\,\varphi \cot(\beta_{2B}) \tag{3}$$

He correlated the coefficients B and C as functions of β_{2B}, Z and R_2/R_1 by solving the potential flow for impellers with logarithmic blade development and constant width. Further investigation of his results revealed that if the radius ratio of R_2/R_1 is greater than $\exp(2\pi \sin(\beta_{2B})/Z)$, then C is equal to 1, and B is only a function of β_{2B} and Z.

Stodola [29] considered the flow between two adjacent blades to be the result of two uniform flows, non-eddy flow and relative eddy, with the eddy velocity equal to the rotational speed of the impeller but in the reverse direction. Considering that the relative eddy flow is the primary mechanism of flow deviation at the impeller outlet and by calculating the circumferential component of the relative eddy flow, he proposed

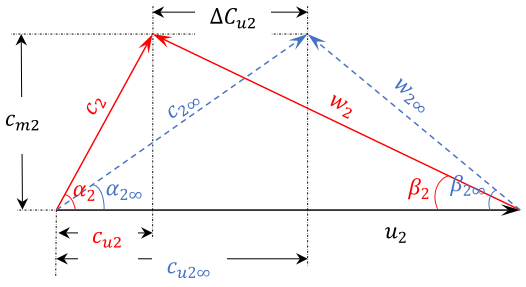

Fig. 1. Velocity triangle at the impeller outlet.

the following model for the prediction of slip factor:

$$\gamma = 1 - \frac{c_{u2\infty} - c_{u2}}{c_{u2\infty}} = 1 - \frac{(\pi/Z)\sin(\beta_{2B})}{1 - \varphi\cot(\beta_{2B})} \tag{4}$$

Based on two-dimensional fluid flow solution in radial impellers, Stanitz [30] suggested the following correlations for predicting slip factor.

$$\gamma = 1 - \frac{0.63\pi}{Z} \tag{5}$$

Later in 1967, Wiesner [25] showed that the model of Busemann [28] is in very good agreement with experimental data and suggested the empirical correlations of Eq. (7) if the ratio of R_2/R_1 is greater than a threshold of ε_{lim} and Eq. (8) if the ratio of radii is less than the threshold.

$$\varepsilon_{lim} = \exp\left(-\frac{8.16\sin(\beta_{2B})}{Z}\right) \tag{6}$$

$$\gamma = 1 - \frac{\sqrt{\sin(\beta_{2B})}}{Z^{0.7}} \tag{7}$$

$$\gamma = \left(1 - \frac{\sqrt{\sin(\beta_{2B})}}{z^{0.7}}\right)\left[1 - \left(\frac{\frac{R_2}{R_1} - \exp\left(8.16\frac{\sin(\beta_{2B})}{Z}\right)}{1 - \exp\left(8.16\frac{\sin(\beta_{2B})}{Z}\right)}\right)^3\right] \tag{8}$$

Gülich [31] adjusted Wiesner's correlation [25] with two additional correction factors:

$$\gamma = f(n_q)\left(1 - \frac{\sqrt{\sin(\beta_{2B})}}{z^{0.7}}\right)k_w \tag{9}$$

$$f(n_q) = \begin{cases} 0.98 & \text{Radial impellers} \\ 1.02 + 0.0012(n_q - 50) & \text{Mixed} - \text{flow impeller} \end{cases} \tag{10}$$

$$k_w = \begin{cases} 1 & d_1/d_2 < \varepsilon_{lim} \\ 1 - \left(\frac{d_1/d_2 - \varepsilon_{lim}}{1 - \varepsilon_{lim}}\right)^3 & d_1/d_2 \geq \varepsilon_{lim} \end{cases} \tag{11}$$

Assuming one single relative eddy in the rotor, Von Backström [32] derived the following unified correlation for slip factor applicable to a wide range of operating conditions of centrifugal impellers:

$$\gamma = 1 - \frac{1}{0.5S\sqrt{\sin(\beta_{2B})}} \tag{12}$$

where S is the solidity and is defined by:

$$S = \frac{1 - \max\left(\frac{R_1}{R_2}, 0.5\right)Z}{2\pi\sin(\beta_{2B})} \tag{13}$$

His correlation unified several validated slip factor models [25,28]–[30,33]. Unfortunately, each of these correlations is valid only for a specific type of impeller and might yield an unrealistic prediction for other types. For example, it was observed [26] that the Stanitz [30] method is not capable of predicting slip factor correctly for impellers with a small number of blades and small blade outlet angles (less than 50°). However, it is one of the best methods for radial impellers with many blades, which is typically the case with radial compressors. In contrast, the prediction obtained with the correlation of Stodola [29] is far from experimental results for impellers having many blades. This correlation is suitable for pumps having a small number of blades and blade outlet angles between 20° and 40°. The Wiesner [25] correlation gives a relatively good result for centrifugal pumps when the ratio of R_2/R_1 is applied within the condition range.

The objective of this work, which is an extension of the results presented in the authors' conference paper [34], is an assessment of the influence of tip clearance on the performance of small-scale turbopumps across a wide range of operating conditions. The variations of the slip factor and the head rise caused by the tip clearance leakage are estimated as a function of influential parameters, providing updated models for considering the tip clearance effect in the early-phase design process of small-scale turbopumps.

2. Methodology

As highlighted in the previous section, due to the lack of suitable and validated reduced-order models for reduced-scale applications, CFD is necessary to obtain a turbopump geometry with acceptable efficiency levels, which can be very time-consuming. To develop new reduced-order models concerning slip and tip clearance losses for the accurate performance prediction of small-scale centrifugal pumps already early in the design process, Neural Network (NN) models fed with CFD data are employed in this work. To build a robust model, diverse training and validation data are required. Therefore, a parametric blade design model is developed and used to generate an extensive range of turbopump geometries for their assessment with a CFD-based approach. The methodology implemented for this work is summarized in Fig. 2.

Given the main dimensions of a turbopump, the meridional profiles of the hub and shroud are necessary to generate the complete geometry and build the blade shape. In conventional approaches, the calculations to achieve the desired profiles involve an iterative process: at first, two arbitrary curves for the hub and shroud are assumed, and once the blade profiles and the impeller design is completed, the cross-sections are evaluated. The curves, the blade profiles and thickness are then changed repeatedly to achieve the desired result. An approach that may not be an optimum solution for automated design. The state-of-the-art approach adopted in this study is developed based on a combination of methods proposed by Zou et al. [35], Wang et al. [36], and Lu et al. [37]. Compared to the classical approach, the advantage is the fact that the meridional shape, which has a dominant effect on flow pattern and performance, is built systematically, i.e., for a chosen area or velocity distribution from the impeller eye to its outlet, which makes it very suitable for the automated generation of different geometries. The medial axis, as depicted in Fig. 3, is the first profile that is generated based on the statistical model developed by Zou et al. [35].

Consider (z, r) as the coordinates of the medial axis curve, s the tangential coordinate along the medial axis, and α the angle, which the tangential coordinate forms with the z-axis in the positive trigonometric direction. z, r, s and α are related as:

$$\frac{dz(s)}{ds} = \cos\alpha(s)$$

$$\frac{dr(s)}{ds} = \sin\alpha(s) \tag{14}$$

Thus, the coordinates of the medial axis curve can be determined as follows:

$$z(s) = z_0 + \int_0^s \frac{dz}{ds}ds = z_0 + \int_0^s \cos\alpha(s)ds$$

$$r(s) = r_0 + \int_0^s \frac{dr}{ds}ds = r_0 + \int_0^s \sin\alpha(s)ds \tag{15}$$

where $r_0 = d_0/2$ and $z_0 = 0$ are known (Fig. 3). Zou et al. [35] suggested that the medial axis can be divided into five segments, and they suggested segments endpoints (Eq. (16)) for a normalized medial axis having a curve length equal to one and being dependent on the specific speed:

$$S_1 = 0$$

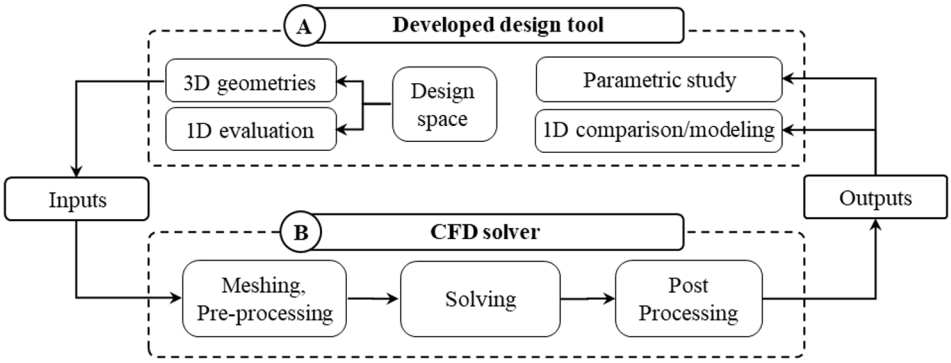

Fig. 2. Methodology flowchart.

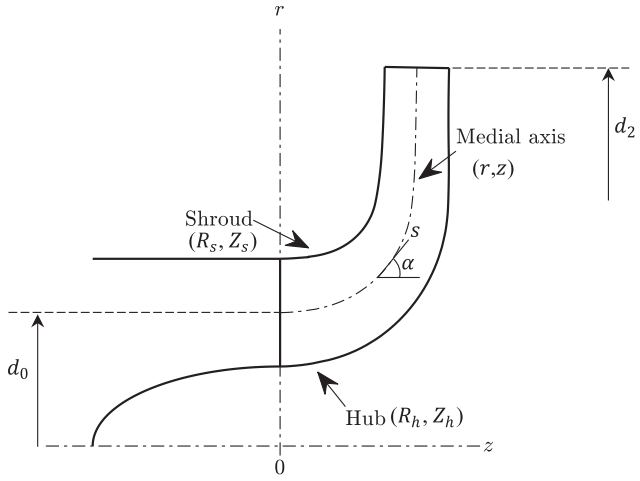

Fig. 3. Meridional profiles: hub, shroud, and medial axis.

$$S_2 = -0.2697e^{-8.748n_s} + 0.1377$$

$$S_3 = -0.5791e^{-2.429n_s} + 0.7477$$

$$S_4 = -0.6175e^{-2.466n_s} + 0.7852$$

$$S_5 = -0.5614e^{-2.544n_s} + 0.9160$$

$$S_6 = 1 \tag{16}$$

where $S = s/L$ is the normalized tangential coordinate and L the medial axis length. For each segment, the angle of the tangent, α, was computed to be:

$$\alpha_1 = 0$$

$$\alpha_2 = -2.1e^{-26.63n_s} + 0.2092$$

$$\alpha_3 = 1.424$$

$$\alpha_4 = 1.467$$

$$\alpha_5 = 1.552$$

$$\alpha_5 = \alpha_6 \tag{17}$$

The (r, z) coordinate of the medial axis can then be calculated by substituting $S = s/L$ (Eq. (16)) and α (Eq. (17)) into Eq. (15) and solving it until the curve length (L) of the medial axis converges to the boundary condition imposed by the outlet diameter of d_2.

In a second step, after the definition of the medial line, the hub and shroud profiles are obtained through a mathematical approach presented by Wang et al. [36] and Lu et al. [37]. Their approach is based on a minimization problem with geometrical constraints on hub and shroud profiles with respect to the generated medial axis (see Fig. 3). The objective function of the minimization problem (Y) is defined with Eq. (18), which unites two equations (Y_1, Y_2) governing the relationship between the curves of hub, shroud, and medial axis:

$$Y(R_s, R_h, Z_s, Z_h) = |Y_1| + |Y_2| \tag{18}$$

$$Y_1 = F(r) - \frac{4}{9}\pi(r + R_h + R_s) \times \left\{ \sqrt{(Z_s - z)^2 + (R_s - r)^2} + \sqrt{(Z_s - Z_h)^2 + (R_s - R_h)^2} \right\} \tag{19}$$

$$Y_2 = \frac{Z_s + Z_h}{2} - z\left(\frac{R_s + R_h}{2}\right) \tag{20}$$

The objective function is dependent on the control points of the medial axis (r, z), the coordinates on the hub (R_h, Z_h) and the coordinates on the shroud (R_s, Z_s). The distribution of the cross-section area ($F(r)$) can be computed with Eq. (21), but it can be given with main design variables such as a chosen area or velocity distribution as Eq. (22), which is the case of this study:

$$F(r) = \frac{4}{9}\pi(R_s + R_h + r)\left\{ \sqrt{(Z_s - z(r))^2 + (R_s - r)^2} + \sqrt{(Z_s - Z_h)^2 + (R_s - R_h)^2} \right\} \tag{21}$$

$$F(r) = \frac{Q}{C_m} \tag{22}$$

The geometrical constraints are presented with Eq. (23) to Eq (25):

$$Z_h = \frac{\{R_s - R_h + 2z(r)z'(r) + (R_s + R_h - 2r)[z'(r)]^2\}}{2z'(r)} \tag{23}$$

$$Z_s = \frac{\{R_h - R_s + 2z(r)z'(r) + (R_s + R_h - 2r)[z'(r)]^2\}}{2z'(r)} \tag{24}$$

$$z \le \frac{Z_s + Z_h}{2} \tag{25}$$

where $z'(r)$ is the derivative of the axial coordinate (z) of the medial axis with respect to its radius (r). The obtained non-linear multivariable optimization problem is solved to compute the four variables R_s, Z_s, R_h and Z_h. Once the main dimensions of the impeller and the meridional profiles are determined, the blade profiles can be computed. The mathematical equations of blade cambers are obtained through the conformal mapping method proposed by Milos [38]. Two parabolic curves as a function of the meridional length (m) with a common tangent at the intersection point, which satisfy the imposed blade angles at the leading edge and trailing edge, represent the blade angle function

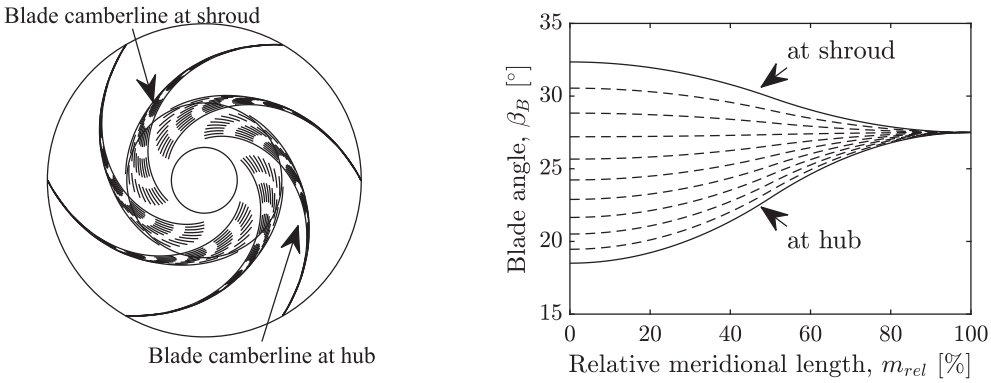

Fig. 4. The blade profiles (left) and their angle development (right) at different spans from the hub to the shroud.

(Fig. 4, right). For each camber line, the leading edge is profiled elliptic, and the transition point from the elliptic profile to the full blade thickness is 5 times the maximum blade thickness. The blade thickness then gradually decreases toward the trailing edge to half of the maximum thickness to reduce pressure fluctuations. The blade is cut off at the trailing edge. The thickness and shape functions are introduced to complete the blade shaping based on considerations suggested by Gülich [31]. To achieve the highest suction performance, the blade is shaped 3D at the leading edge (LE), and it has been converted to 2D at the trailing edge (TE) for easier manufacturing (see Fig. 4). The imposed area distribution, imposed blade angle curve and leading-edge shape are defined with the best engineering practice so that the pressure drop at the vicinity of the blade leading edge is minimal, leading to a higher margin against cavitation.

The blade profiles can be mapped back from the conformal mapping plan to the streamline surfaces represented with the cylindrical coordinates (r, θ, z). The blade surfaces can then be visualized using an appropriate script giving the blade geometry (Fig. 5).

Numerical scheme. The parametric blade design tool is employed to automatically generate turbopump geometries within the parametric ranges listed in Table 1 using a factorial design approach, leading to 72 shrouded and 504 unshrouded designs to be assessed with CFD. The diversity of the analyzed turbopump geometries is illustrated in Fig. 6. On average, each impeller geometry is obtained with the automated design tool within 15.8 s with a serial (single core) calculation on a workstation running with an Intel Xeon processor (E5-1650 v3 3.50 GHz). Solving the minimization problem to find the hub and shroud curves takes up most of the runtime. The angle definition is shown in Fig. 1, and the clearance gaps are normalized based on the blade outlet width. The design parameters are selected based on the requirements of an ORC system with a net output power of 8 kW for waste heat recovery applications on truck engines and running with R245fa as a working fluid [5,39]. The corresponding pump needs to be able to deliver a pressure rise of 28 bar and a mass flow of 0.28 kg/s at the design point. The scaling is based on Buckingham's Pi-theorem, and the fluid is R245fa with density and dynamic viscosity of 1311.9 kg.m^{-3} and 3.525 $\times$ 10^{-4} Pa.s, respectively, at the inlet conditions.

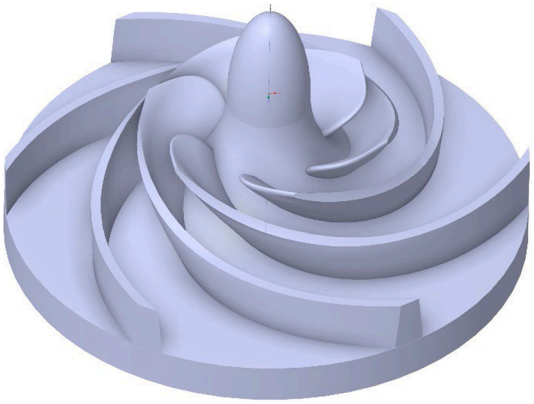

Fig. 5. 3-d representations of a blade geometry.

Table 1
Parametric ranges of ORC turbopumps.

Outlet diameter	13, 16, 18, 24	(mm)
Blade angle	15, 22.5, 27.5, 32, 50, 90	(°)
No. blades	5, 6, 7	(–)
Tip clearance ratio	0.05, 0.1, 0.15, 0.2, 0.3, 0.4, 0.6	(–)
Rotational speed	40, 50, 63.5, 75	(krpm)
Reynolds number	$1.2 \times 10^6 - 2.3 \times 10^6$	(–)

In order to assess and analyze the performance and detailed flow patterns of the different turbopumps, the geometries are evaluated with CFD. The computational domain consists of an inlet duct and an impeller. The inlet duct length is 10 times the impeller diameter and is meshed with a hexahedral structured grid with an expansion ratio of 1.8. A structured mesh with a global size factor of 1.20 is adopted for the impeller, leading to meshes with 800,000 to 1,500,000 elements. Table 2 provides details of the computation grid for studying turbopump range specified in Table 1.

Boundary layer treatment and near-wall elements are controlled based on y^+ evaluation to ensure their values lie in the range of the turbulence model validity (Mentor [40]). The mesh of the tip clearance gap is constructed with a fine grid with more than 45 layers with an end ratio of 30 to 43. The sizing is based on initial manual evaluation and mesh independence at the edges of the range of the parameters. The grid independence is confirmed for two turbopumps with blade outlet angles of 22.5° and 90°. Grids with different size factors are generated so that the simulation is converged, and the static and total pressure rises achieve a steady state. A comparison of the total pressure rise against various grid sizes is carried out and represented in Fig. 7. The total pressure rise starts to plateau at a grid size factor of about 1.05. A very high grid size factor leads to a very fine mesh, which may cause the solver's failure due to numerical instability and accumulations of errors. Therefore, the grids with a global size factor of 1.20, which lead to mesh independent results, are selected in this study.

At the inlet and outlet, the total inlet pressure and the mass flow rate are set, respectively. The walls are treated with no-slip and rough conditions. The turbulence is modeled with Mentor's shear stress transport model [40] due to its capability in the prediction of separation and secondary flows in rotary domains. The rough wall condition moves the logarithmic velocity profile closer to the wall and influences the efficiency, especially in small-scale applications. Therefore, its influence is accounted for in the near-wall treatment of the turbulence model. The time-averaged equations of mass and momentum assuming steady-state

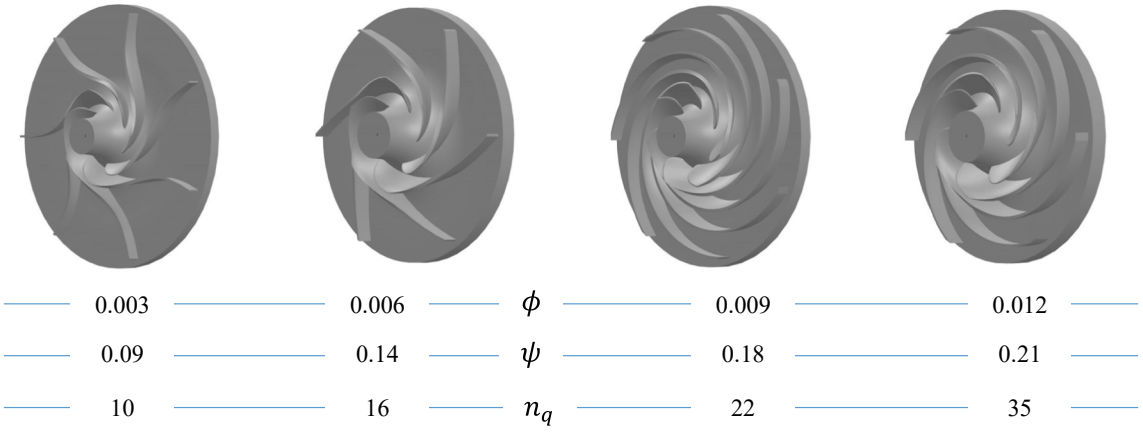

Fig. 6. The diversity of studying turbopumps (values are post-computed).

Table 2
The specifications of the computational grid.

Parameter	Setting
Global size factor	1.20
Inlet growth ratio	1.80
Maximum expansion rate	1.30
Boundary layer specification	Reynolds number and first element y^+
Reynolds number	Set based on blade chord
Vertex offset specification mode	y^+
First element y^+	< 2

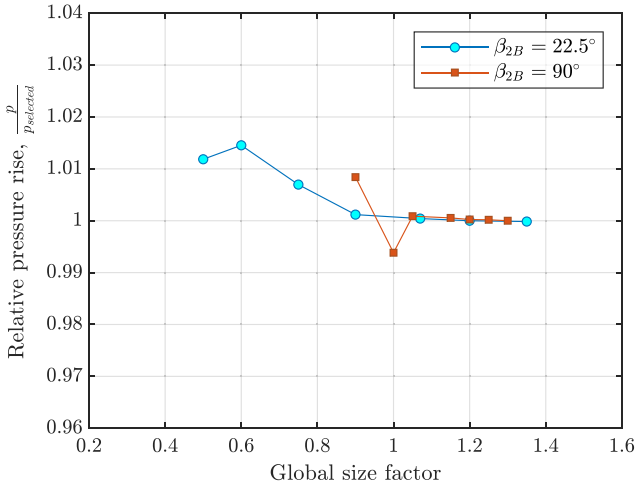

Fig. 7. Grids independence study for two studied turbopumps.

condition and incompressible flow are solved numerically with the CFX solver. Overall characteristics such as head rise, efficiency, and flow conditions at the outlet converge after approximately 150 iterations. Although only the overall characteristics are considered for the results of this study, simulations are conducted for a minimum of 400 iterations, even if the residuals are less than the convergence criteria, which is set to an RMS residual target of 10^{-5}. The developed tool shown in Fig. 2 propagates the problem to six workstations running on Intel Xeon Processor E5-1650 v3 3.50 GHz.

3. Results and discussion

The results obtained from the numerical approach enable the characterization of performance indicators, such as slip factor, efficiency, head coefficient and head loss due to tip clearance. Though the results are only carried out for R245fa, the findings can be used in the design of centrifugal pumps running with other fluids as long as the non-dimensional parameters summarized in Fig. 6 and Table 1 are respected.

3.1. Slip factor

Shrouded impellers. In Fig. 8, the slip factors computed based on CFD results and the corresponding estimations predicted by well-known correlations are shown for shrouded impellers designed for running at 50,000 rpm. Von Backström [32] and Wiesner [25] correlations provide the best agreement with the CFD results. However, as the blade angle increases, the accuracy of both models decreases. The Von Backström [32] correlation seems closer to CFD data than the Wiesner [25] correlation. The Stanitz [30] correlation, although developed for radial impellers ($\beta_{2B} = 90°$), fails to predict the slip factor also for purely radial designs. It was highlighted, however, that when the number of blades is small, the estimations predicted by the Stanitz [30] correlation are not accurate.

The CFD results of Fig. 8 are replotted in Fig. 9 to highlight the variation of the slip factor with blade outlet angle and the number of blades and to illustrate the comparison between Von Backström's [32] correlation and CFD results for the shrouded impeller. The CFD data suggest that at a constant number of blades, the slip factor initially decreases and then increases with increasing blade angle β_{2B}, with a minimum at a β_{2B} of 50°. This is a trend, that is not captured with conventional correlations, e.g., Von Backström [32], as shown in Fig. 9. Contours and vectors of normalized relative velocity (w/u2) around the blades are shown in Fig. 10. The figure highlights vortices causing severe flow deviation at the TE growing with β_{2B}, thus emphasizing the increase of the slip factor with β_{2B}.

Considering the data presented in Fig. 8 and Fig. 9 are only subsets, Fig. 11 summarizes the relative deviations of slip factors predicted by correlations compared to CFD data for all shrouded impellers. Relative error (e_i) and mean relative errors ($\bar{e}$) as well as standard deviation (σ) defined by Eq. (26) to Eq. (28), respectively, are considered for the evaluation of the different correlations:

$$e_i = \frac{\left|X_{predicted_i} - X_{CFD_i}\right|}{X_{CFD_i}} \times 100 \tag{26}$$

$$\bar{e} = \frac{1}{n}\sum_1^n e_i \tag{27}$$

$$\sigma = \sqrt{\frac{1}{n}\sum_1^n (e_i - \bar{e})^2} \tag{28}$$

As the plots suggest, the Von Backström [32] correlation provides the best agreement with CFD data, predicting 100 % of the values within a

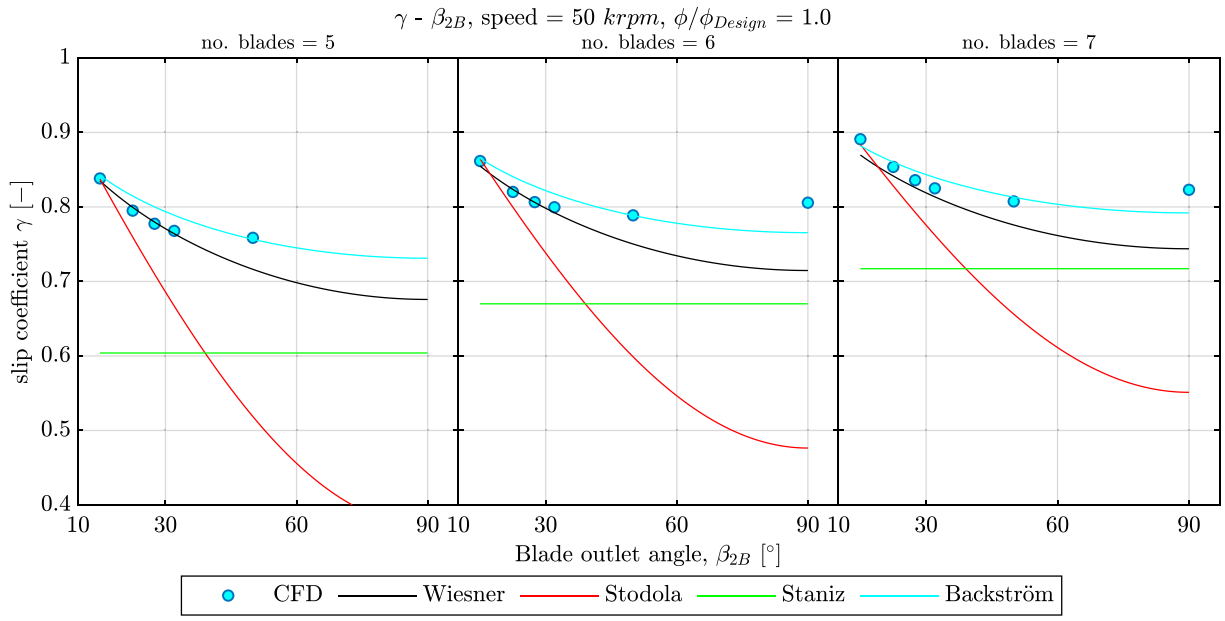

Fig. 8. Comparison between slip factors computed based on CFD results and correlation estimations for shrouded impellers.

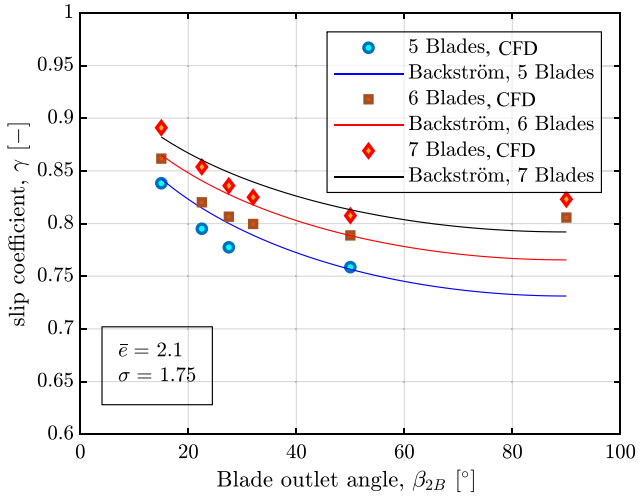

Fig. 9. Change of slip factors with blade outlet angle and number of blades in comparison to prediction achieved with Von Backström [32] correlation (shrouded impellers).

relative deviation of ± 10 %. The correlation of Wiesner [25] is the second most accurate method, with 90.1 % of the predicted values within a relative deviation of ± 10 %. The comparison with correlations of Stodola [29] and Stanitz [30] shows that only 2 % and 60 % of the predictions are within ± 10 % relative deviation, which is not satisfactory. The very good agreement between CFD results for shrouded impellers with the well-known correlations of Von Backström [32] and Wiesner [25] validates the methodology and accuracy of CFD results as the mean relative difference and standard deviation calculated to be 2.1 % and 1.75 % respectively for Von Backström's [32] correlation.

Unshrouded impellers. Fig. 12 presents the slip factors calculated based on CFD results for different blade outlet angles and the number of blades for unshrouded impellers designed for 40,000 rpm and operating at their design flow rate. For each design, the corresponding value of the shrouded impeller is represented with a blue circle. While the slip factor values vary significantly with tip clearance, they follow almost the same trend as shrouded impellers, namely decreasing and then increasing with β_{2B}.

It is expected that a higher deviation from CFD results would be observed when correlations are applied to unshrouded impellers. The comparison between the model prediction for unshrouded impellers and CFD data is represented in Fig. 13. According to the results, the slip factors predicted with Von Backström's [32] and Wiesner's [25] correlations deviate by ± 20 % compared to CFD data. The relative deviation is much higher for Stodola [29] and Stanitz [30].

In Fig. 14, the slip factors are plotted against β_{2B} for shrouded and selected unshrouded impellers with a tip clearance ratio of 0.2 for various mass flows, suggesting that the slip factor is less dependent on the flow rate at a larger blade outlet angle. This corroborates with the conclusion of one-dimensional perfect flow analysis, where the theoretical head rise is independent of the operating flow rate [31]. Referring to Fig. 10, at a larger β_{2B}, the core flow is influenced more profoundly by secondary flows, even at the design point. Therefore, additional flow disturbance induced by off-design operation seems to have a lower influence on velocity components at the TE, and therefore the slip factor is less influenced by the flow rate. A similar observation has been reported by Ishida et al. [17] for centrifugal compressors.

Fig. 15 presents the slip factor as a function of the relative flow coefficient for various discharge blade angles and tip clearance ratios. The data suggests the slip factor decreases as the flow coefficient increases for both shrouded and unshrouded impellers. This decrement, however, varies between shrouded and unshrouded impellers, with a more pronounced effect for unshrouded impellers (represented by squares in the figure).

The slip factors are plotted against tip clearance ratios for design mass flow operation in Fig. 16. The 0-value on the x-axis corresponds to shrouded impellers. The results indicate that the variation of slip factor against tip clearance ratio is not linear and increases for small ratios of tip clearance (<0.10) and then decreases to reach minimum values at intermediate tip clearance ratios before rising again for very large tip clearances. The tip leakage flow driven by the pressure difference between the pressure and suction side of the blade enters the core passage flow with a different streamwise velocity component. The consequent mixing results in the generation of vortices within the core flow passage and thereby changes velocity components and the velocity triangle significantly, as demonstrated in the literature [19]. Concisely, the slip factor decreases with increasing β_{2B} and rises with the number of blades.

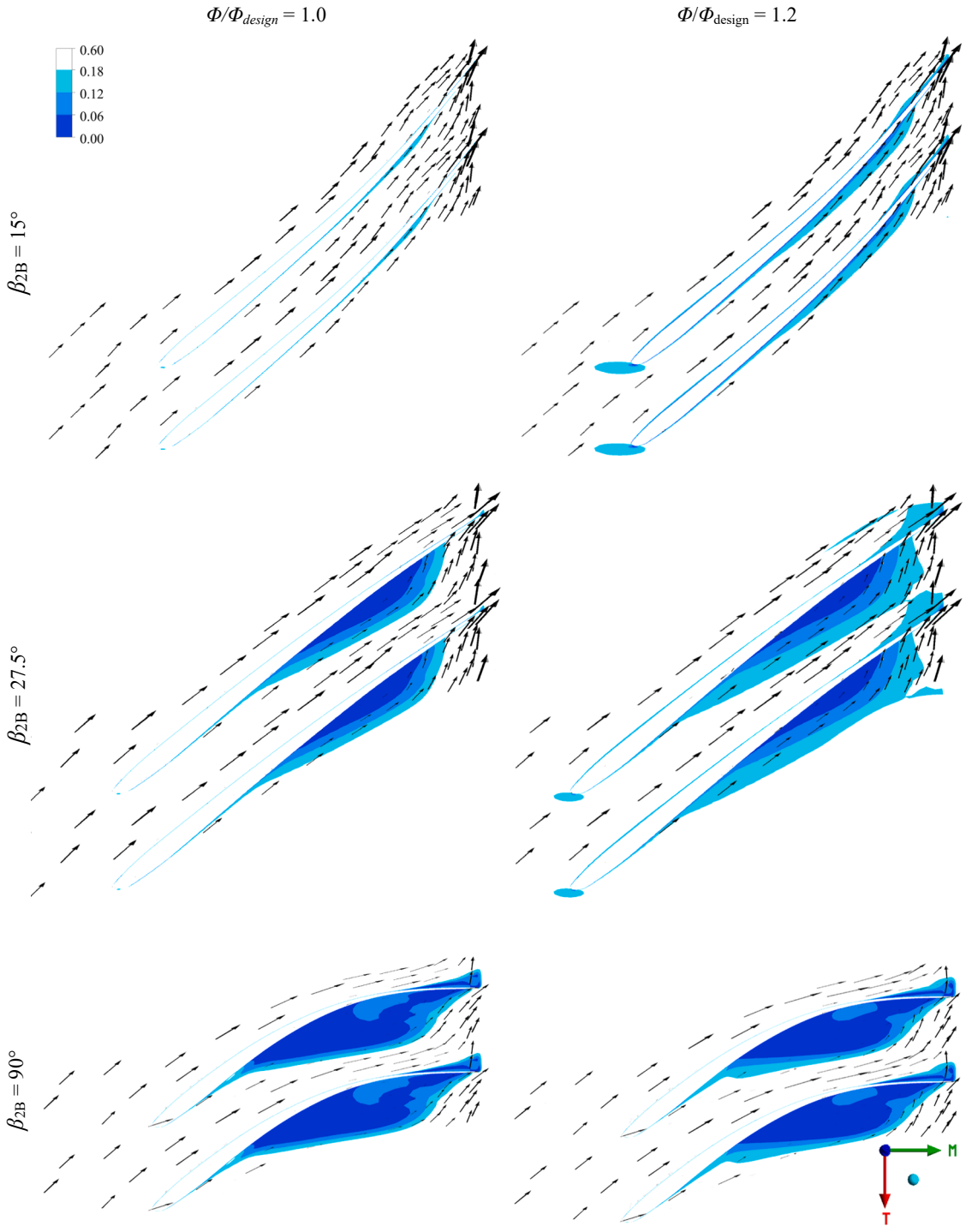

Fig. 10. Contours and vectors of normalized velocity (w/u_2) at mid-span for shrouded impellers.

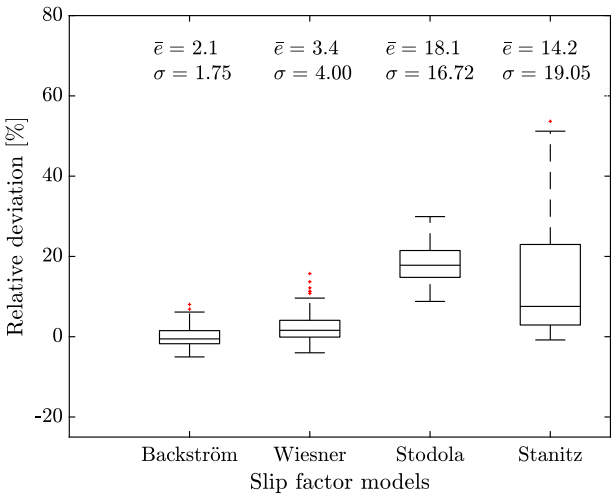

Fig. 11. Relative deviation of slip factors predicted with correlations compared to CFD data for all shrouded impellers.

3.2. Performance reduction due to the tip clearance

The overall performance is computed for all studied cases, and the performance maps in terms of head coefficient against flow coefficient for different blade outlet angles and tip clearance ratios are summarized in Fig. 17. The data suggests that the apparent head rise decrement due to the tip clearance is strongly dependent on the blade outlet angle and on the tip clearance ratio. The larger the tip clearance ratio, the larger the apparent head rise decrement. On the other hand, the apparent head reduction decreases with increasing blade outlet angle. Hence, the head coefficient for impellers with a more radial blade is suggested to be less sensitive to tip clearance. The impeller with purely radial blades (outlet angle of 90°) shows interesting performance characteristics. For small tip clearance ratios of 0.05 and 0.10, the head coefficients of unshrouded impellers are higher compared to a shrouded impeller. Nevertheless, the unshrouded ones exhibit more than 20 % less efficiency at tip clearance ratios of 0.05 and 0.10, as shown in Fig. 18.

In Fig. 18, the impeller efficiency is plotted as a function of the relative flow coefficient at different tip clearance ratios and six different blade angles. The efficiency is computed as follows:

$$\eta = 100 \times \frac{\rho Q g H_{in\ to\ out}}{P_{shaft}} \tag{29}$$

For each blade angle, the efficiency is found to reach its minimum value at the largest tip clearance, which is in agreement with the literature. The slope of the efficiency drop with the relative flow coefficient varies both with the blade outlet angle and the tip clearance ratios. The slope becomes steeper with increasing tip clearance. Also, the lower the blade outlet angle, the higher the efficiency drop slope.

Influence of parameters on performance reduction. As pointed out previously, the tip clearance reduces the impeller Euler head. Thus, the tip clearance influences the impeller head rise through both the reduction of input work and the head loss. Therefore, the head loss can be written as:

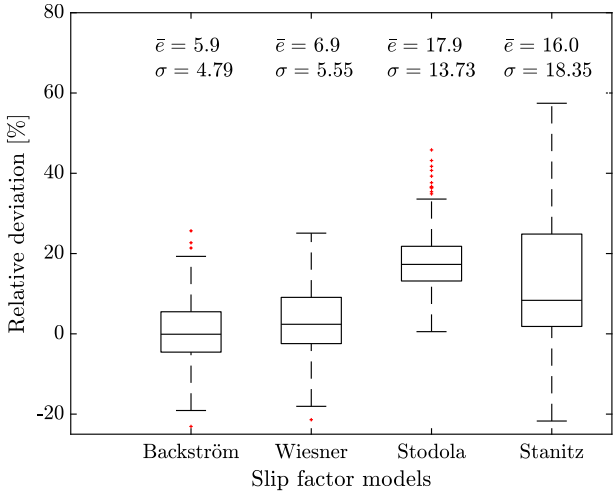

Fig. 13. Relative deviation of slip factors predicted with correlations compared to CFD data for all unshrouded impellers.

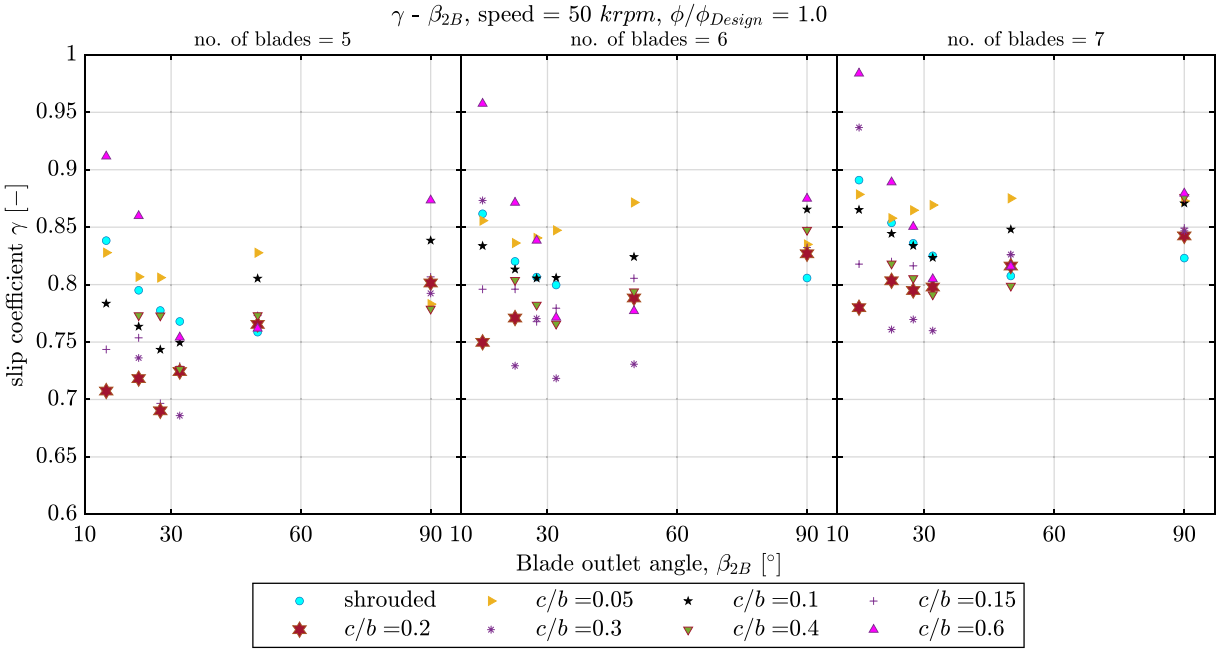

Fig. 12. Change of slip factors with tip clearance ratios and blade outlet angles at different numbers of blades.

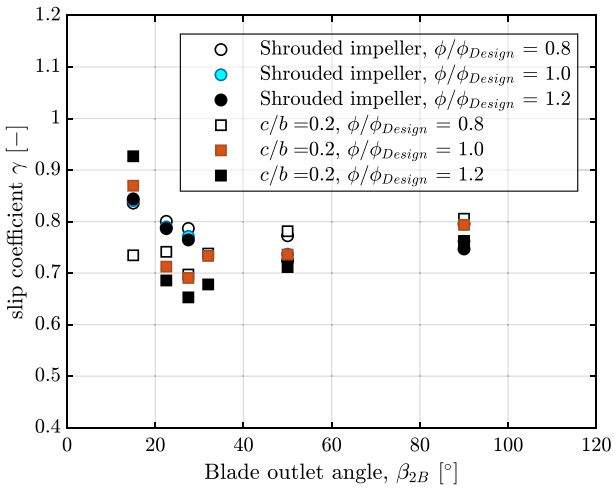

Fig. 14. Effect of blade outlet angle on slip factor at different flow rates.

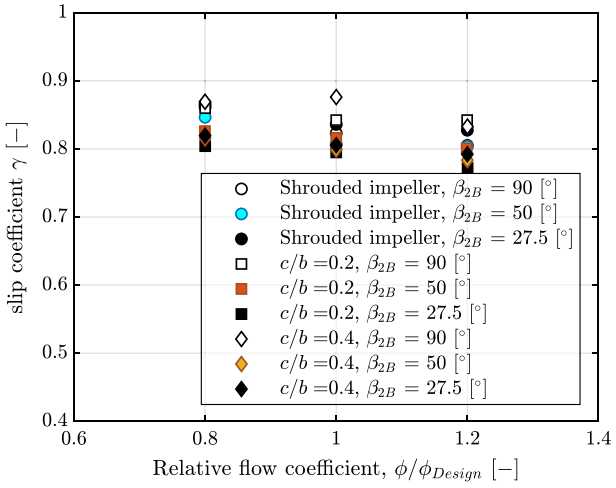

Fig. 15. Effect of flow rate on slip factor of impellers with different blade angles.

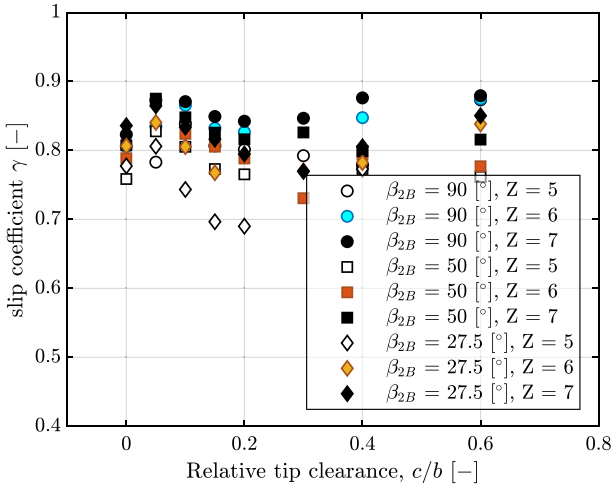

Fig. 16. Effects of tip clearance ratios on the slip factor.

$$\psi_{loss} = (\psi_0 - \psi) - (\psi_{i0} - \psi_i) \tag{30}$$

where the first parenthesis corresponds to the apparent head rise decrement and the second one to the input work difference.

Fig. 19 shows the influence of the blade outlet angle on the head loss coefficient for two tip clearance ratios of 0.1 and 0.2 at different flow rates. The head loss coefficients are normalized based on the input head coefficient of the base shrouded impeller. The relative head loss coefficient diminishes with increasing β_{2B} for all tip clearances and flow rates.

The influence of tip clearance ratios on the relative head loss coefficient is shown in Fig. 20. The relative head loss coefficient initially rises rapidly as the tip clearance ratios increase and then flattens. The linear variation of hydraulic losses induced by the tip clearance at low tip clearances is also observed by Diehl et al. [24] for radial compressors. The change of the slope varies greatly with β_{2B} and decreases for smaller tip clearance ratios and higher β_{2B}. The high dependency of head loss coefficient to the tip clearance at smaller tip clearance ratios is analogous to the finding of Brasz [15] on radial compressors. Further, the results indicate that the number of blades has little impact on the head loss induced by the tip clearance. The negative values of the relative head loss coefficient in Fig. 20 correspond to radial blade impellers with a very small tip clearance. Referring to Fig. 17, the head coefficients of such impellers are higher compared to corresponding shrouded impellers.

Fig. 21 presents the non-dimensional stagnation pressure contour at the impeller outlet (defined in Eq. (31) and Eq. (32)). With increasing tip clearance ratios, the minimum reduced stagnation pressure decreases, and the region with minimum values grows. This effect is more pronounced for lower β_{2B}. At larger tip clearance ratios, more flow leaks through the tip clearance and does not get mixed entirely with the main flow. Consequently, the reduced stagnation pressure decreases.

$$p_{T,\,red} = p_S + \frac{\rho}{2}\left(w^2 - u^2\right) \tag{31}$$

$$C_{p_{T,red}} = \frac{p_{T,\,red} - \overline{p_{T,\,red,\,in}}}{\rho u^2} \tag{32}$$

3.3. Neural network model

To obtain more reliable prediction models for the slip and the head loss coefficient due to tip clearance, two neural network (NN) based surrogate models have been implemented. Although available models were correlated based on experimental data, the NN models of this study are trained on a much large number and a wider range of data points. Building a NN model consists of three essential steps. The process starts with obtaining training and test data. Training data is a subset of data that the NN model uses to learn how to solve the problem, while test data is a subset of data never seen by the NN model used to evaluate the accuracy of the model and to avoid overfitting. The data used to train the slip factor model is obtained based on the parametric ranges listed in Table 1. 100 unshrouded impellers and their equivalent shrouded cases (required for the tip loss model) are randomly generated and solved with CFD, which is then used for testing the generated NN models. Test impellers do not share any common parameter with the training data and were randomly generated and used to evaluate the model. Hence, the test data is independent of the training data, except that both were evaluated using the same CFD setup.

The second step is selecting the appropriate learning algorithm. Through an iterative process, the optimal structure of the NN is found. The process consists of executing input variables through the algorithm, evaluating how well the model is doing given the training data, and then adjusting the weights and biases of neurons in the algorithm to achieve the most accurate prediction. The neuron is a sum of a weighted average of its input and a constant term called bias unit. Weights determine the influence of each input on the next layer, while bias units, which are independent of the previous layer, guarantee the neuron can still get

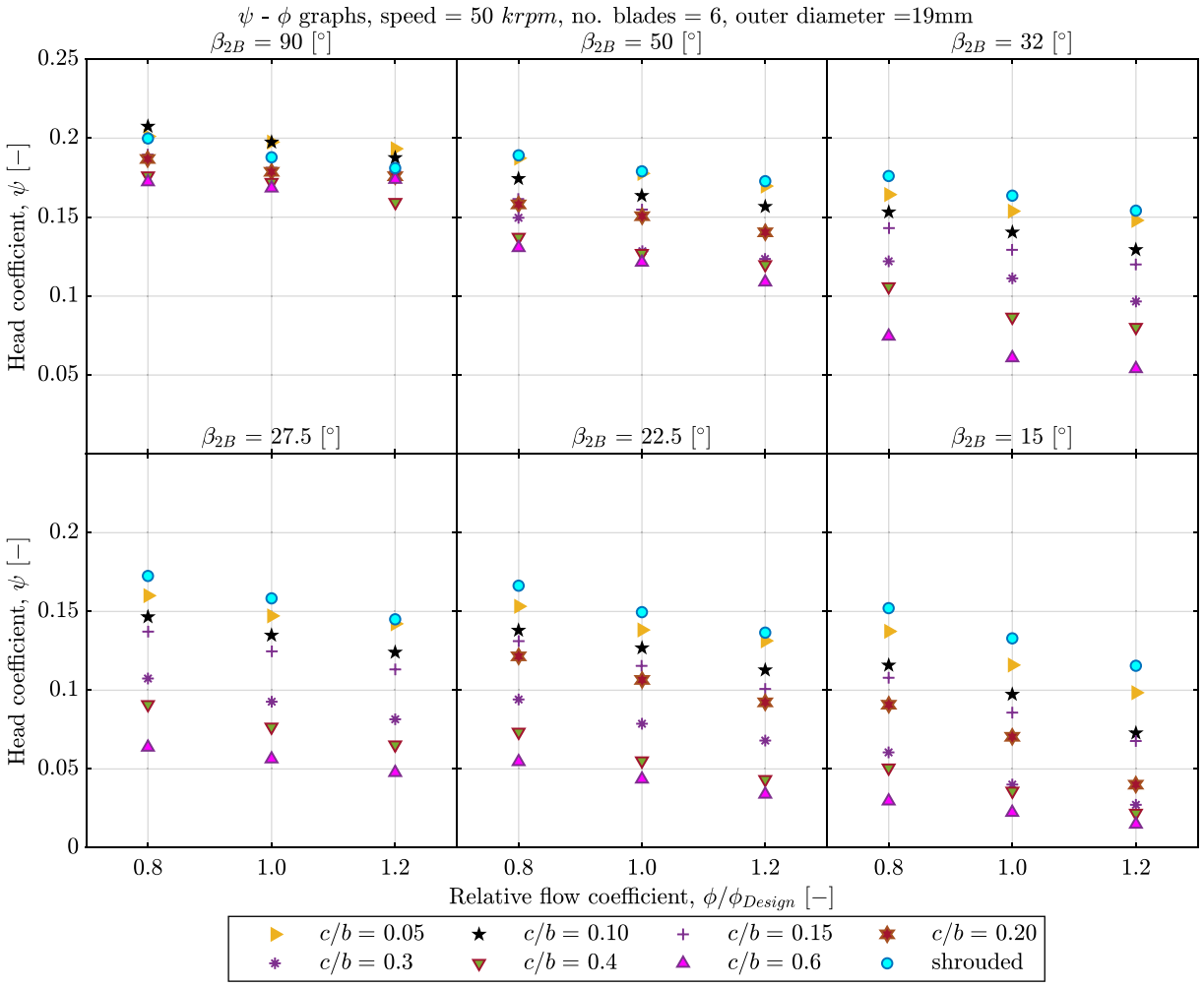

Fig. 17. Performance map ($\psi - \phi$) of unshrouded impellers with different blade outlet angles in comparison to their respective base shrouded impeller.

activated even if all the inputs are zero. The sum is passed through a non-linear function called the activation function. The neuron values on each layer can be computed as (See Fig. 22):

$$Z_i = W^{(i)}(\sigma(Z_{i-1})) + b^{(i)} = W^{(i)}h_{i-1} + b^{(i)} \tag{33}$$

where σ and h are the activation function applied to the previous layer and its output, respectively. The objective function is the mean square error of predicted values of training data and is described as Eq. (34), in which m is the number of training data.

$$J(\Theta) = \frac{1}{2m}\sum_{i=1}^{m}\left(y_{CFD}^{(i)} - y^{(i)}\right)^2 \tag{34}$$

The neural network of this research is implemented using Flux [41] in the environment of the Julia programming language [42]. The core feature of Flux is the adoption of native Julia code to take gradients, which results in significantly lower computation time. The tip clearance ratio, β_{2B}, number of blades, β_{le}, the ratio of the inlet to outlet diameters, and the specific speed were taken as input parameters for the head loss coefficient model, while the first three parameters and the flow coefficient were inputs for the slip factor model.

For the slip factor, the best algorithm is determined to be a feed-forward neural network with two hidden layers of 5 neurons, each with a sigmoid activation function. Fig. 23 presents the relative deviation of slip factors predicted with the NN model for the training and test data. The NN model predicts 100 % of both training and test CFD data within a relative deviation of ± 10 %, yielding an average absolute deviation of 1.6 % and 3.6 % for training and test data, respectively. Compared to 83 % of data predicted within ± 10 % relative deviation by Von Backström [32] correlation, the NN model improves the prediction accuracy of slip factors significantly.

For the head loss coefficient, the optimized NN design consists of two hidden layers with 15 neurons each, with a sigmoid activation function. 100 % of CFD data are predicted within a relative deviation of ± 10 %, as shown in Fig. 24. Therefore, the NN models are capable of properly mapping arbitrary input data into their correct target values for the slip factor and head loss coefficient for small-scale turbopumps.

The parameters of the final optimized neural network designs can be accessible from the respective data repository of the study [43]. The importance of NN modeling can be realized when the CFD data are compared with other models. Hence the relative head loss coefficients calculated based on CFD results are compared with the corresponding

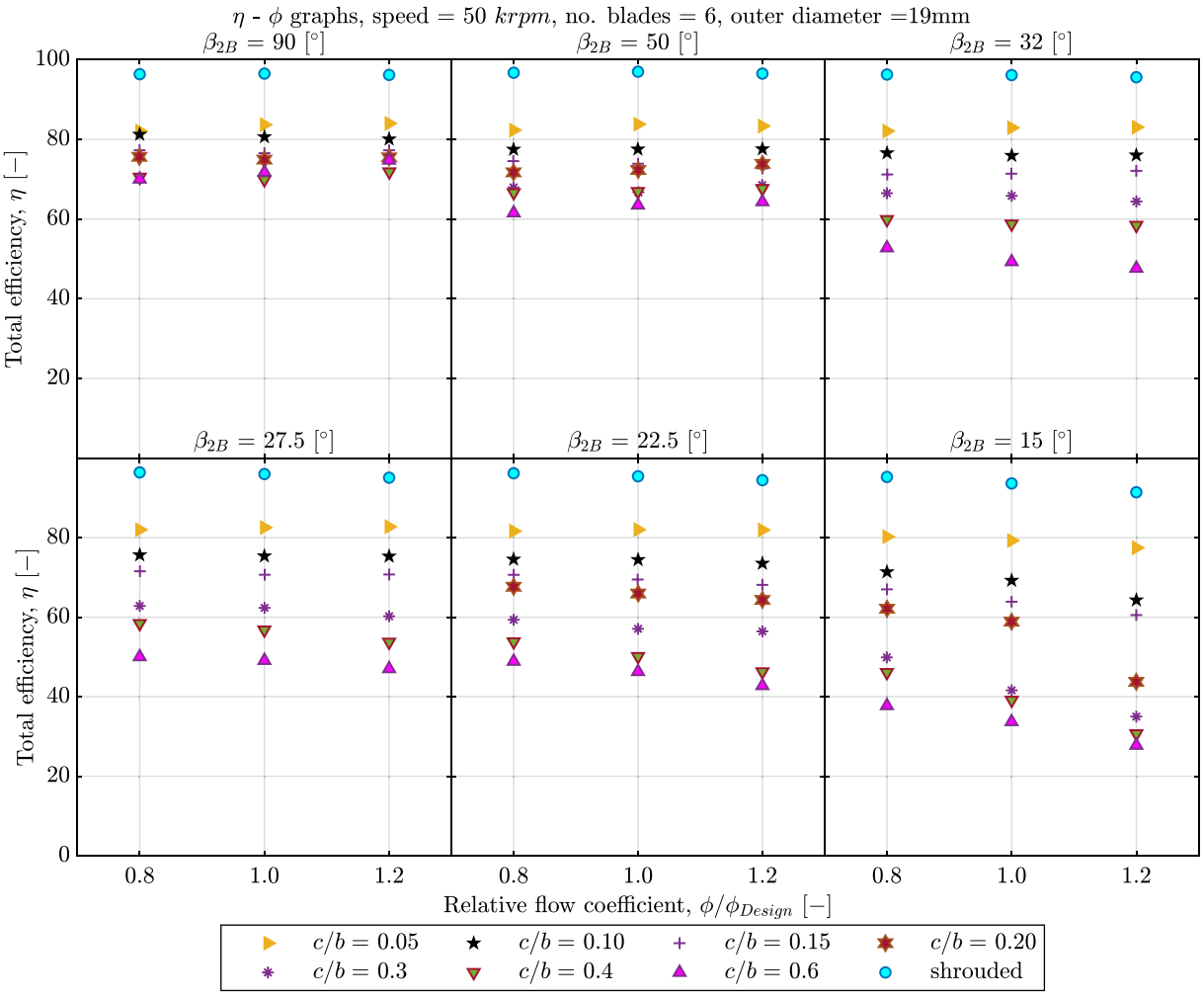

Fig. 18. Efficiency plots ($\eta - \phi$) of unshrouded impellers with different blade outlet angles in comparison to their respective base shrouded impeller.

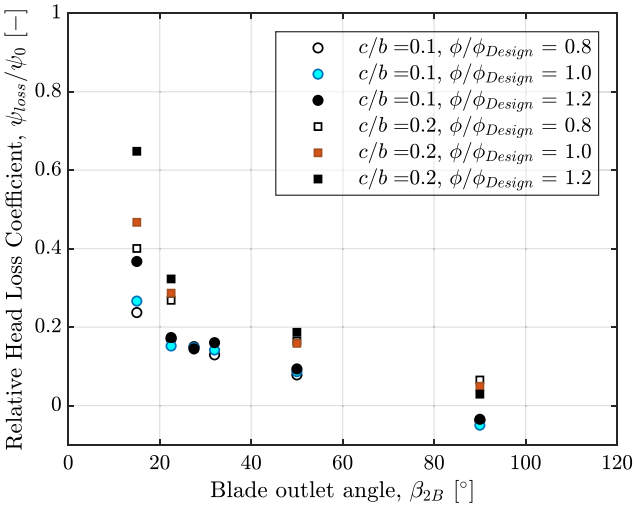

Fig. 19. Effect of blade outlet angle on relative head loss coefficient.

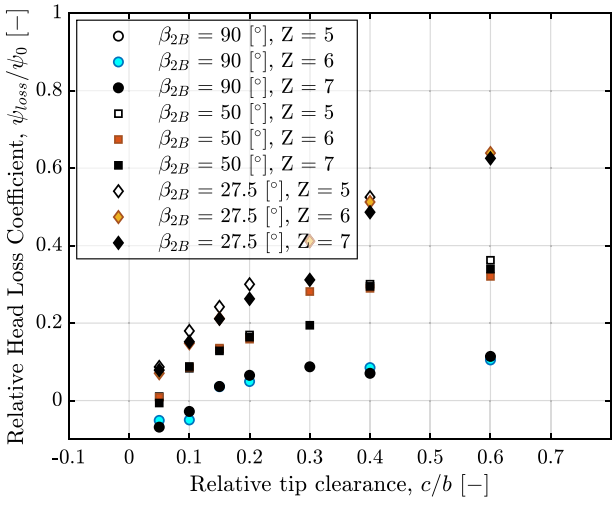

Fig. 20. Effect of tip clearance ratios on relative head loss coefficient.

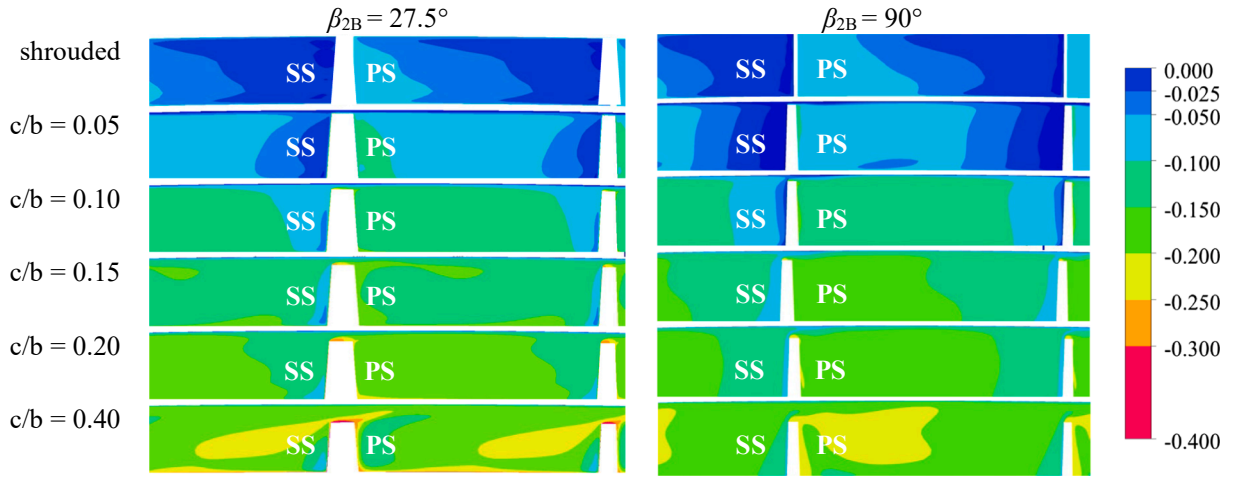

Fig. 21. Contours of non-dimensional stagnation pressure contour ($C_{P_{t_r}}$) at the impeller outlet.

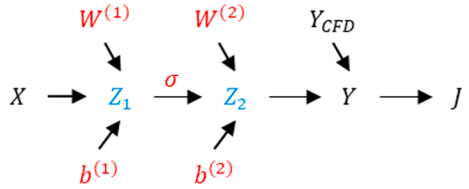

Fig. 22. General neural network architecture.

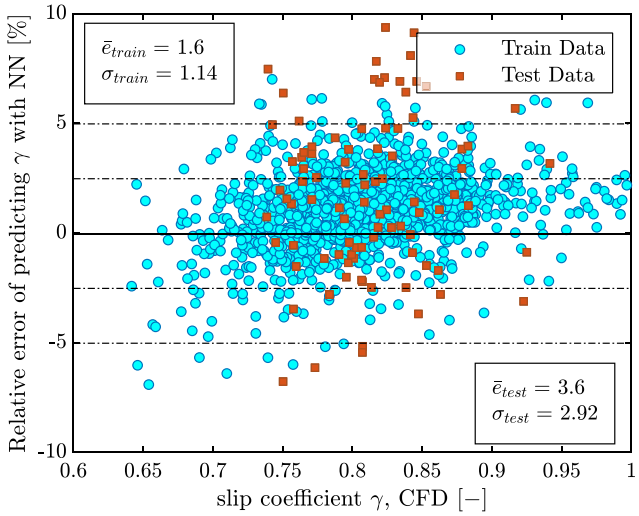

Fig. 23. Relative deviation of slip factor predicted with NN from CFD results.

values estimated with the correlation provided by Gülich [31] in Fig. 25. The correlation is presented in Table 3. The scatter of the data points suggests that the correlation is not capable of predicting the relative head loss coefficients of turbopumps operating in the scope of this study.

Although the model of Gülich [31] is not able to predict the relative head loss coefficient, it may be possible to achieve better estimations by a non-linear regression analysis using the same correlation structure. In Fig. 26, the relative tip head loss coefficient calculated based on CFD results is compared against the corresponding values predicted by the new non-linear regression model as presented in Table 3. The proposed model predicts 73 % and 92 % of CFD results within ± 10 % and ± 20 % relative deviation limits, respectively, which improves the prediction accuracy significantly compared to the Gülich correlation.

As summarized in Table 3, the average absolute deviation and the

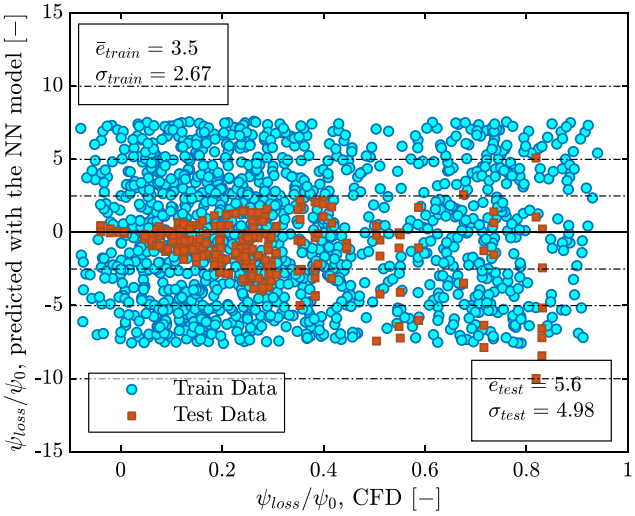

Fig. 24. Relative deviation of head loss coefficient predicted with NN from CFD results.

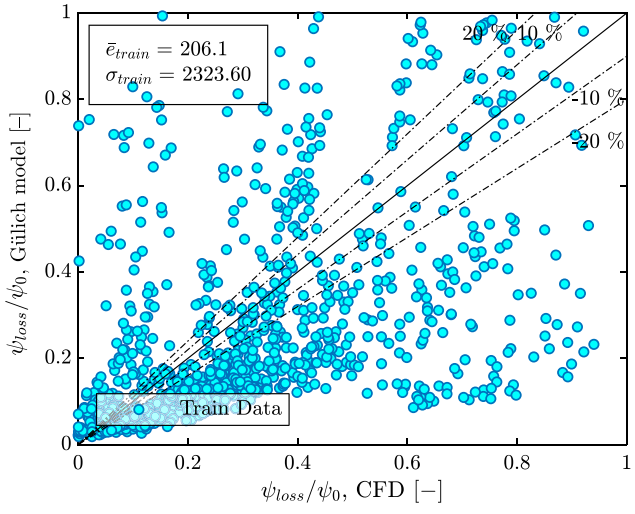

Fig. 25. Relative deviation of head loss coefficient predicted with the correlation of Gülich [31] from CFD results.

Table 3
Accuracy of models predicting head loss coefficient.

Model	Formula	$\bar{e}$(%)	σ(%)	±10 % (%)	±20 % (%)
Gülich [31]	$\frac{\Delta\psi}{\psi_0} = \frac{2.5c/d_2}{\sqrt{\frac{b_2}{d_2}\left(1-\frac{d_1}{d_2}\right)Z\left(\frac{e}{t_2}\right)^{0.2}} n_q^{1.2} \sin(\beta_2)^{0.4} \sin(\beta_2)}$	206.1	2323.6	42	45
Non-linear	$\frac{\Delta\psi}{\psi_0} = \frac{0.465 n_q^{0.051} (c/b)^{0.483} (d_1/d_2)^{0.383}}{\sin(\beta_1)^{0.142} \sin(\beta_2)^{0.834} Z^{0.053}}$	189.2	1894.4	73	92
NN	$Z_i = W^{(i)}(\sigma(Z_{i-1})) + b^{(i)} = W^{(i)} h_{i-1} + b^{(i)}$	5.4	4.6	100	100

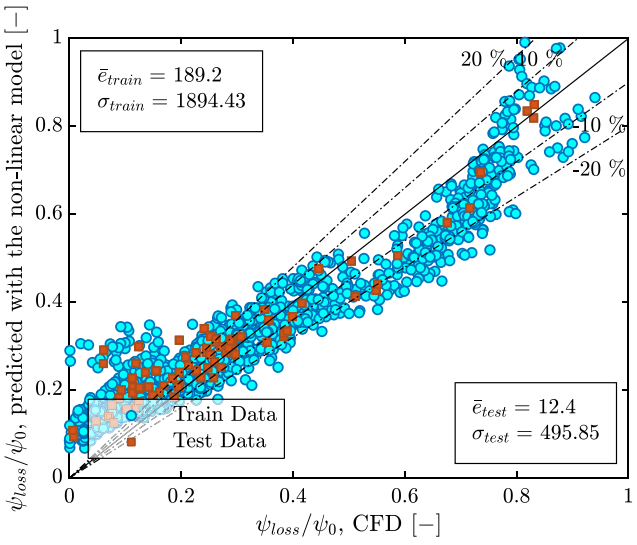

Fig. 26. Relative deviation of head loss coefficient predicted with the non-linear correlation from CFD results.

standard deviation decreased respectively from 189.2 % and 1894.4 % for the non-linear regression model to 5.6 % and 4.98 % with the neural network model. This suggests that the NN model can improve the prediction accuracy of turbopump performance significantly.

4. Conclusions

A new robust and automated design model was developed to generate 920 different impellers of small-scale turbopumps for ORC, covering a wide range of geometrical parameters with specific speeds ranging from 10 to 35. The influence of tip clearance, β_{2B}, number of blades, and flow rate on performance at design and off-design conditions are investigated and modeled. The key findings of this work can be summarized as follows:

1. The CFD data suggest that the slip factor of centrifugal pumps is dependent not only on their geometrical parameters, as considered by most correlations, but also on their operating conditions. The slip factor is suggested to decrease linearly with the flow rate.
2. The tip clearance influences the slip factor non-linearly. At high β_{2B} (radial impellers), the effects of tip clearance and flow rate on the slip factor diminish.
3. The head rise decreases with the tip clearance ratio. However, for radial impellers, a higher head rise was observed for small tip clearance ratios (<0.1). More investigation should be carried out to understand the underlying mechanisms leading to this observation.
4. The effect of tip clearance flow leads to complex flow patterns, and a simple model cannot accurately consider the influential parameters affecting the slip factor and performance of an unshrouded impeller.
5. Feedforward neural networks were trained to model the influence of dominant parameters on the slip factor and head loss coefficient of unshrouded impellers. The models can be applied to predict the tip clearance effects on the performance of centrifugal turbopumps if the non-dimensional parameters in Fig. 6 and Table 1 are met. The surrogate models predict the CFD data with an average relative deviation of 3.6 and 5.8 % for the slip factor and the head loss coefficient, respectively. Thus, the models successfully improve the performance prediction accuracy of centrifugal pumps in an early design phase.

Declaration of Competing Interest

The authors declare that they have no known competing financial interests or personal relationships that could have appeared to influence the work reported in this paper.

Data availability

The parameters of the final optimized neural network designs can be accessible from the respective data repository of the study

References

[1] D. Serrano *et al.*, Improving train energy efficiency by Organic Rankine Cycle (ORC) for recovering waste heat from exhaust gas, 2015.
[2] F. Meng, H. Zhang, F. Yang, X. Hou, B. Lei, L. Zhang, Y. Wu, J. Wang, Z. Shi, Study of efficiency of a multistage centrifugal pump used in engine waste heat recovery application, Appl. Therm. Eng. 110 (2017) 779–786.
[3] A. Landelle, N. Tauveron, R. Revellin, P. Haberschill, S. Colasson, V. Roussel, Performance investigation of reciprocating pump running with organic fluid for organic Rankine cycle, Appl. Therm. Eng. 113 (Feb. 2017) 962–969, https://doi.org/10.1016/j.applthermaleng.2016.11.096.
[4] G. Bianchi, F. Fatigati, S. Murgia, R. Cipollone, Design and analysis of a sliding vane pump for waste heat to power conversion systems using organic fluids, Appl. Therm. Eng. 124 (2017) 1038–1048, https://doi.org/10.1016/j.applthermaleng.2017.06.083.
[5] K. Rosset, V. Mounier, E. Guenat, J. Schiffmann, Multi-objective optimization of turbo-ORC systems for waste heat recovery on passenger car engines, Energy 159 (2018) 751–765.
[6] K. Rosset, O. Pajot, J. Schiffmann, Experimental investigation of a small-scale organic rankine cycle turbo-generator supported on gas-lubricated bearings, J. Eng. Gas Turbines Power 143 (5) (2021), https://doi.org/10.1115/1.4049988/1097002.
[7] G.M. Wood, H. Welna, R.P. Lamers, Tip-clearance effects in centrifugal pumps, J. Fluids Eng., Trans. ASME 87 (4) (1965) 932–939, https://doi.org/10.1115/1.3650846.
[8] R.C. Pampreen, Small turbomachinery compressor and fan aerodynamics, J. Eng. Gas Turbines Power 95 (3) (1973) 251–256, https://doi.org/10.1115/1.3445730.
[9] J.A. Block, P.W. Runstadler, Effect of Specific Heat Ratio, Impeller Tip Running Clearance, and Compressor Insulation on High-Pressure-Ratio Centrifugal Compressor Modeling, Am. Soc. Mech. Eng. (Paper) (75-Fe-9) (1975) 9–14.
[10] T. Mashimo, I. Watanabe, I. Ariga, Effects of Fluid Leakage on Performance of a Centrifugal Compressor, Am. Soc. Mech. Eng. (Paper) 101 (78-GT-143) (1978) 337–342.
[11] M. Ishida, Y. Senoo, On the pressure losses due to the tip clearance of centrifugal blowers, vol. 103, no. 80, 1980, pp. 271–278, doi: 10.1115/80-gt-139.

[12] Y. Senoo, M. Ishida, Pressure loss due to the tip-clearance of impeller blades in centrifugal and axial blowers, vol. 108, no. (Lecture Ser. 1984-07), 1984.
[13] Y. Senoo, M. Ishida, Deterioration of compressor performance due to tip clearance of centrifugal impellers, J. Turbomach. 109 (1) (1987) 55–61, https://doi.org/10.1115/1.3262070.
[14] A. Engeda, M. Rautenberg, Comparisons of the Relative Effect of Tip Clearance on Centrifugal Impellers, Am. Soc. Mech. Eng. (Paper) 109 (October) (1987) 1–5.
[15] J.J. Brasz, Investigation into the effect of tip clearance on centrifugal compressor performance, Proc. ASME Turbo Expo 1 (1988) 1988, https://doi.org/10.1115/88-GT-190.
[16] M. Ishida, H. Ueki, Y. Senoo, Effect of blade tip configuration on tip clearance loss of a centrifugal impeller, *Proc. ASME Turbo Expo* 1(89) (1989). doi: 10.1115/89GT80.
[17] M. Ishida, Y. Senoo, H. Ueki, Secondary flow due to the tip clearance at the exit of centrifugal impellers, Proc. ASME Turbo Expo 1 (January) (1989) 19–24, https://doi.org/10.1115/89GT81.
[18] A. Goto, Study of internal flows in a mixed-flow pump impeller at various tip clearances using 3D viscous flow computations, Proc. ASME Turbo Expo 1 (90) (1990) 373–382, https://doi.org/10.1115/90-GT-036.
[19] S. Aknouche, Impact of Tip Clearance Flow on Centrifugal Pump Impeller Performance by Sebastien Aknouche, 2003. [Online]. Available: dspace.mit.edu/handle/1721.1/82254.
[20] H.J. Eum, Y.S. Kang, S.H. Kang, Tip clearance effect on through-flow and performance of a centrifugal compressor, KSME Int. J. 18 (6) (2004) 979–989, https://doi.org/10.1007/BF02990870.
[21] J. Tang, T. Turunen-saaresti, A. Reunanen, J. Honkatukia, J. Larjola, Numerical Investigation of the Effect of Tip Clearance to the Performance of a Small Centrifugal Compressor, 2006, pp. 1–8.
[22] A. Jaatinen, T. Turunen-Saaresti, A. Grönman, P. Röyttä, J. Backman, Experimental study of the effect of the tip clearance to the diffuser flow field and stage performance of a centrifugal compressor, *Proc. ASME Turbo Expo*, 8(PARTS A, B, AND C) (2012) 641–648. doi: 10.1115/GT2012-68445.
[23] Q. Sun, Y. Gong, Q. Li, Effect of Tip Clearance Flow on the Evaluation of Slip Factor for Micro Impellers, 2012, pp. 1–7.
[24] M. Diehl, C. Schreiber, J. Schiffmann, The Role of Reynolds Number Effect and Tip Leakage in Compressor Geometry Scaling at Low Turbulent Reynolds Numbers, J. Turbomach. 142 (3) (2020), https://doi.org/10.1115/1.4045465.
[25] F.J. Wiesner, A Review of Slip Factors for Centrifugal Impellers, J. Eng. Gas Turbines Power 89 (4) (1967) 558–566.
[26] M. Memardezfouli, A. Nourbakhsh, Experimental investigation of slip factors in centrifugal pumps, Exp. Therm Fluid Sci. 33 (5) (2009) 938–945, https://doi.org/10.1016/j.expthermflusci.2009.03.011.
[27] A. Stepanoff, Centrifugal and axial flow pumps: theory, design, and application, Wiley, New York, 1957.
[28] A. Busemann, Das Förderhöhenverhältnis radialer Kreiselpumpen mit logarithmisch-spiraligen Schaufeln, ZAMM-Journal of Applied Mathematics and Mechanics/Zeitschrift für Angewandte Mathematik und Mechanik 8 (5) (1928) 372–384.
[29] A. Stodola, Steam and gas turbines: with a supplement on the prospects of the thermal prime mover, vol. 2, McGraw-Hill, 1927.
[30] J.D. Stanitz, Some theoretical aerodynamic investigations of impellers in radial and mixed flow centrifugal compressors, Trans. ASME 74 (4) (1952) 473–497.
[31] J. Gülich, *Centrifugal pumps*, Springer, Berlin, Heidelberg, 2010. Accessed: Jul. 01, 2019. [Online]. Available: https://link.springer.com/content/pdf/10.1007/978-3-540-73695-0.pdf.
[32] T. von Backström, A Unified Correlation for Slip Factor in Centrifugal Impellers, *J. Turbomach.-Trans. ASME* 128 (2006). doi: 10.1115/1.2101853.
[33] B. Eck, Fans, 1st English ed.., Pergamon Press, Oxford, 1973, pp. 139–153.
[34] S. Zakeralhoseini, J.A. Schiffmann, The effects of the tip clearance on the performance of small-scale turbopumps for ORC applications; analysis and modeling, in: *Proceedings of the 6th International Seminar on ORC Power Systems*, 2021, vol. 2021, no. 112. [Online]. Available: http://infoscience.epfl.ch/record/289985.
[35] J. Zou, P. Wang, X. Ruan, X. Fu, A Statistical Method on Meridional Profiles of Centrifugal Pumps, J. Fluids Eng. 134 (2) (2012), 024502, https://doi.org/10.1115/1.4005667.
[36] Y. Wang, Q. Dong, Y. Zhang, Meridional shape design and the internal flow investigation of centrifugal impeller, Proc. Inst. Mech. Eng., Part C: J. Mech. Eng. Sci. 231 (23) (2017) 4319–4330, https://doi.org/10.1177/0954406216667407.
[37] Y. Lu, X. Wang, R. Xie, Derivation of the Mathematical Approach to the Radial Pump's Meridional Channel Design Based on the Controlment of the Medial Axis, Math. Probl. Eng. 2017 (2017) 1–15, https://doi.org/10.1155/2017/7027016.
[38] T. Miloş, CAD Procedure For Blade Design of Centrifugal Pump Impeller Using Conformal Mapping Method, Fifth Conference of the Water-Power Engineering in Romania, Published in Scientific Bulletin of University POLITEHNICA of Bucharest, Series D, Mechanical Engineering 70 (4) (2008) 213–220.
[39] K. Rosset, O. Pajot, J. Schiffmann, Experimental Investigation of a Small-Scale Organic Rankine Cycle Turbo-Generator Supported on Gas-Lubricated Bearings, 1–14,51015, J. Eng. Gas Turbines Power 143 (5) (2021), https://doi.org/10.1115/1.4049988.
[40] F. Menter, M. Kuntz, R.B. Langtry, Ten years of industrial experience with the SST turbulence model, Heat Mass Transf. 4 (2003).
[41] M. Innes, Flux: Elegant Machine Learning with Julia, J. Open Source Software (2018), https://doi.org/10.21105/joss.00602.
[42] J. Bezanson, S. Karpinski, V.B. Shah, A. Edelman, Julia: A fast dynamic language for technical computing, *arXiv preprint arXiv:1209.5145*, 2012.
[43] S. Zakeralhoseini, J. Schiffmann, Neural network models for centrifugal pumps, Mendely Data (2022).